Tumor characterization using the backscatter coefficient at low and high-frequency

Cyril Malinet, Celia Mansilla, Iveta Fajnorova, Adrien Rohfritsch, David Melodelima, Aurélie Dutour, Pauline Muleki Seya

Tumor characterization using the backscatter coefficient at low and high-frequency

1st Cyril Malinet
CREATIS, CNRS, INSERM
Villeurbanne, France

2nd Celia Mansilla
CREATIS, CNRS, INSERM
Villeurbanne, France
celia.mansilla@creatis.insa-lyon.fr

3rd Iveta Fajnorovà
CRCL / CLB
Lyon, France

4th Adrien Rohfritsh
LabTAU, INSERM
Lyon, France
adrien.rohfritsch@inserm.fr

5th David Melodelima
LabTAU, INSERM
Lyon, France
devid.melodelima@inserm.fr

6rd Aurélie Dutour
CRCL / CLB
Lyon, France
aurelie.dutour@lyon.unicancer.fr

7rd Pauline Muleki-Seya
CREATIS, CNRS, INSERM
Villeurbanne, France
pauline.muleki-seya@creatis.insa-lyon.fr

***Abstract*—The backscatter coefficient (BSC) is an interesting parameter for cancer characterization. In this study, we investigated the interest of evaluating the BSC at high (40MHz) and low (15Mz) frequencies for characterizing ex vivo sarcomas. The agreement of BSCs at high and low frequencies for chondrosarcomas suggests the same scattering structure at these two frequencies (probably nuclei or cells). The mismatch for osteosarcomas would indicate a different scattering structure in these two cases with nuclei as scatterers at high frequency. These results show the value of scanning at low and high frequencies for characterizing these tumors.**

***Index Terms*—Cancer characterization, Backscatter coefficient, Sarcomas**

I. Introduction

Cancer is the main cause of death in France, just ahead of cardiovascular diseases. The examination that will allow the diagnosis to be made to characterize a tumor is the biopsy. However, this exam remains an invasive and highly localized procedure. Ultrasound imaging is particularly interesting to try to characterize a cancer because it is a safe modality allowing to image the entire tumor fastly and painlessly and this modality is accessible worldwide. Ultrasonic Backscatter Coefficient (BSC) can quantify tissue microstructure properties non-invasively [1]. BSC quantitative technique provides system and operator-independent information about the scattering structures in a tissue. This technique and the derived parameter from the BSC have been used to differentiate cancer from healthy tissue, as in the case of prostate [2] and lymph nodes [3]. Oelze et al. [4] showed that it was also possible to differentiate a benign from a malignant tumors. More recently, we have shown that this technique can differentiate chondrosarcoma from osteosarcoma ex vivo in rodent models [5]. Tumors are not necessarily homogeneous because of the presence of vascularization, for example, but also because of the presence in some tumors of large-scale structures such as acini or lobules. This study aims to evaluate whether there is an interest in performing US measurements at both low and high frequencies while characterizing these kinds of tumors to access scattering from different structures for example.

This work was supported by Canceropole CLARA under grant OS14-25-CAMUT

II. Material and methods

A. Theoretical BSC

The Fluid-Filled Sphere model describes tissue as an ensemble of monodisperse discrete scatterers with impedance differing from that of a homogeneous background medium. The structure factor model (SFM) is based on the assumption that, at high scatterer volume fractions, interference effects are mainly caused by correlations between the spatial positions of individual scatterers that can be modeled with the structure factor. The theoretical BSC formulation for the SFM model (SFMm) is given by [6]. It depends on the scatterer radius a, the volume fraction ϕ, and the relative impedance contrast γ_Z.

As the scatterer are not often monodisperse, the polydisperse model was introduced. An expression of polydisperse BSC in the case of concentrated medium required the expression of a structure factor for polydisperse scatterer that can be found in [7]. In this model, the scatterer size distribution is assumed to follow a Γ-distribution. The theoretical BSC formulation for this polydisperse BSC model (SFMp) depends on the scatterer mean radius a and Schulz factor ζ (describing the shape of the scatterer size distribution), the volume fraction ϕ, and the relative impedance contrast γ_Z.

B. Animal models

The experiment was conducted on chondrosarcomas (CHS) and osteosarcomas (OSA) in agreement with the European and French regulations and was approved by the ethical committees ACCESS and CECAPP (registration number C2EA15 for CHS and 35086 for OSA). All tumor implantations were performed on anesthetized animals. CHS

tumors were transplanted into 25-day-old Sprague-Dawley rats as described before by [8]. The OSA model were established by injection of $1{\times}10^6$ K7M2 suspended cells [9] in the tibia of 11 BALB/cByJ mice. Upon establishment of palpable tumors (vol 50 mm^3). Rats and mice were scanned over 3 weeks or till tumors reached max ethical volume 2500 mm^3 or 600 mm^3, respectively, using a sequential euthanasia protocol. CHS and OSA Tumor growth was monitored by measurement of tumor volume with a caliper twice a week. ultrasonic measurements were realized immediately after euthanasia and tumor removal.

C. Ultrasound Measurements

Ultrasound measurements were conducted at high frequency (Vevo 770, RMV704, f_c=40 MHz) and at low frequency (Verasonics, L228 probe, f_c=15 MHz). Eleven ex vivo osteosarcomas and 12 chondrosarcomas were scanned at 40 MHz and on 4 of these osteosarcomas and 5 chondrosarcomas were scanned at 15 MHz. At least 10 scans per tumor were acquired at high frequency and 5 scans at low frequency.

BSCs were computed using the phantom reference technique (ROI of 15 λ (RMV704) and 10 λ (L228) in both direction). RMV704 probe has a fixed focal depth at 6 mm, the interface of the tumor was placed just above this focal depth and mostly the first millimeter of the tumor was imaged. This strategy was chosen to image always the same position whatever the tumor size. A plane wave strategy (13 angles from -5°to 5°) was preferred for the L228 probe acquisition. The entire tumor was scanned. The ROIs were located in homogeneous regions in the first millimeter of the tumors (RMV704) or the entire tumor (L228). A diagram of the area in which ROIs have been defined for the two probes is presented in Figure 1. Non-overlapping ROI were used for the high frequency acquisition and 75% overlapping for low frequency were less ROI could be obtained otherwise. A signal-to-noise ratio (SNR) criterion was applied to filter out ROIs with noisy power spectra for the high frequency [5]. It mainly remove the ROI to far from the focal line.

The attenuation coefficients were estimated following the standard substitution methods [10] for each tumor. The BSC for each ROI was estimated using the reference phantom method [11]. Our reference phantom was composed of polyamide particles of diameter 5 μm (Orgasol 2001 UD, Arkema) at the relative mass concentration of 0.25 % in a gel that contains agarose (2%, Sigma) and water. The BSC of the reference phantom was computed using the Faran theory. A mean BSC per tumor was obtained by averaging BSCs values from all ROIs in a given tumor.

D. Histological analysis

After ultrasound imaging, histological analysis was realized on 5 μm formalin-fixed paraffin-embedded on an automated

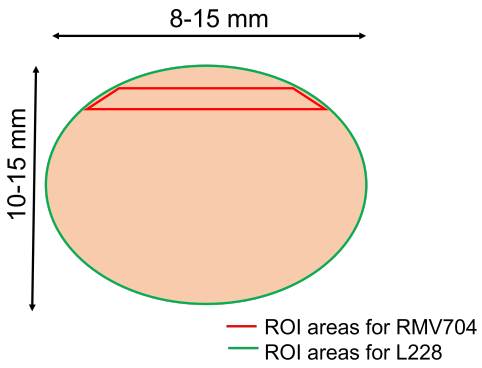

Fig. 1. Example of Bmode images obtained with RMV704 (a) and L228 (b). (c) Diagram of the area in which ROIs have been defined for these two probes.

Ventana Discovery ULTRA staining system (Ventana Medical Systems, Tucson, Az, USA). OSA cells and nuclei size distribution were estimated automatically with QuPath (software version 0.3.2). For CHS, a manual segmentation was used to estimate the size distributions of cells and nuclei using ImageJ (v.1.52a, Waynes Rasband National Institutes of Health, USA). Cell segmentation was performed in areas corresponding to the ROIs where ultrasound acquisitions were realized (i.e. maximum depth = 1 mm) on the part of the tumor corresponding to the top of ultrasound acquisitions (regions greater than 0.4 mm^2). The radii of cells and nuclei were extracted by assuming the circularity of the detected objects. Nucleus and cell mean values, Schulz factors and their surface fractions estimated for each tumor of the same kind were averaged to be used as input variables for the theoretical monodisperse and polydisperse BSC models.

III. Results

A. Histological analysis

Classical structures for CHS and OSA models are observed on histological images. OSA tumors are heterogeneous with the presence of areas of dense cell proliferation and areas of necrosis (Fig 2(a)). At a smaller scale, OSA model is characterized by high cellular density of small cells with large nuclei (Fig 2(b)). CHS tumors show the presence of lobules but are rather homogeneous (Fig 2(c)). CHS is characterized by low cell density of large cell with small nuclei within an abundant extracellular matrix (Fig 2(d)). One can clearly distinguish the extracellular membrane, cell cytoplasm and cell nuclei.

The cells and nuclei radius distribution estimated from histological images were presented in Figure 3. Because the nuclei and cell radius detections were automatic for OSA, there were more of them, and the results for nucleus and cell sizes, as well as surface fractions, are more reliable compare to CHS. However, the distributions for different tumors of the same tumor type give rather close size distributions. The

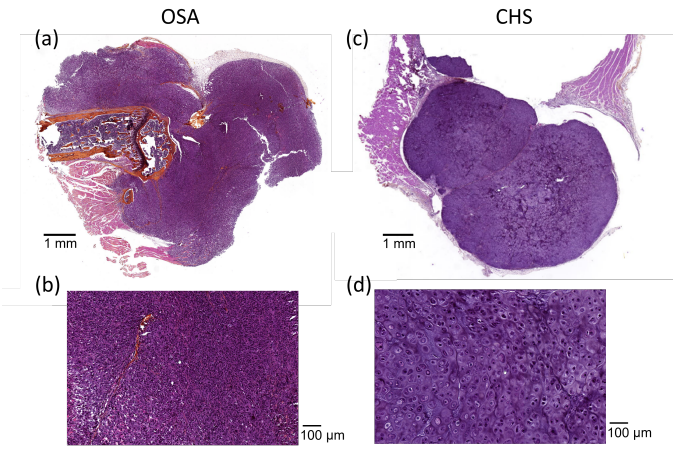

Fig. 2. Example of histological images obtained for OSA (a-b) and CHS (c-d).

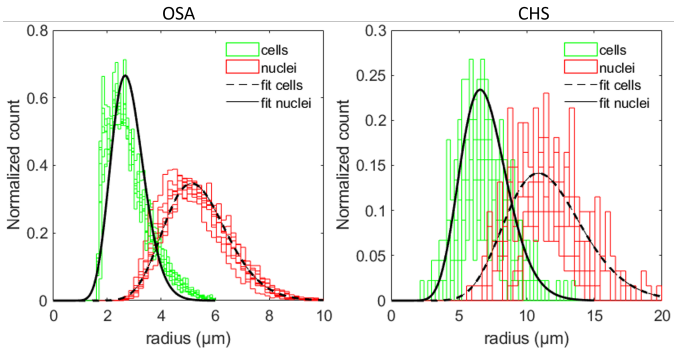

Fig. 3. OSA and CHS cells and nuclei distribution from histology and a fitted distribution from a Gamma distribution.

average radius and cell values obtained are summarized in Table 1. The cell and nuclear radius distributions were fitted by a gamma distribution (Fig 3) and Schulz factors, which describe the variance of the distribution, of 20 (OSA) and 15 (CHS) were retained. The cell and nuclear surface fractions for OSA and CHS are summarized in Table 1. The radius results and surface fractions obtained are quite close to the results from a previous study on the same models [5], except for the CHS cell surface fraction. Since this surface fraction is really very low, a surface fraction value of 0.25, close to the surface fraction from [5] was used for the estimation of theoretical BSCs. For the theoretical BSC, as an approximation the volume fractions for cells and nuclei were assumed equal to the surface fractions [12].

B. BSC analysis

Mean BSCs for each CHS and OSA tumors at low and high frequencies are presented in Figure 4(a-b). For CHS experimental mean BSCs at low and high frequencies are in agreement but not for OSA.

In the literature, the acoustic impedance of cells (nuclei/cytoplasm) has been estimated or measured to

	OSA	CHS
mean cell radius (μm)	5.4	11.6
mean nucleus radius (μm)	2.8	7.0
Schulz factor ζ	20	15
mean cell surface fraction	0.90	0.08 (0.25 used)
mean nucleus surface fraction	0.26	0.03

TABLE I
SUMMARY OF CELL AND NUCLEUS RADIUS AND SURFACE FRACTION ESTIMATED FROM HISTOLOGY FOR OSA AND CHS WITH THE SCHULZ FACTOR ESTIMATED FROM THE SIZE DISTRIBUTIONS.

be around 1.6 MRay [13], [14], that of collagen-based tissue between 1.6 and 1.9 MRay [13] and that of cartilage between 2.1 and 2.3 MRay [15]. Based on these values, a maximum relative impedance contrast, γ_Z, around 0.3 is expected.

For CHS, theoretical BSC using SFMm and SFMp for nuclei are concordant with measured BSCs (Fig 4(a). Theoretical BSC using SFMp for cells is also concordant with experimental BSCs but shows a less good agreement than theoretical BSCs for the nucleus. For OSA, theoretical BSC using SFMm and SFMp for nuclei are concordant with high-frequency measured BSCs as well as theoretical BSC using SFMp for cells but for a too high relative impedance contrast value (γ_Z=0.55) (Fig 4(b).

IV. DISCUSSION

The good agreement between low- and high-frequency BSC for CHS tumors may reflect that the same structure is involved in ultrasound scattering at both low- and high-frequency and/or that CHS are homogeneous tumors, allowing homogeneous ROIs even if they have different sizes and different locations in the tumor (Fig 1). By comparing the experimental BSC with theoretical ones using values from histology, our CHS results suggest a scattering from nuclei or cells for CHS (Fig 4(a).

The lack of agreement between low- and high-frequency BSC for OSA tumors may reflect that the structure involved in ultrasound scattering at low and high frequencies are different and/or that OSA are more heterogeneous tumors, providing different BSC in the region scanned at low and high frequency. Large areas of necrotic core were not observed in the OSA tumors in this study. The main difference between the peripheral zone (the only zone scanned at high frequency) and the central zone (also scanned and averaged at low frequency) could be a difference in cell proliferation between these zones and therefore a difference in the volume fraction of the scatterers. However, a difference in scatterer volume fraction does not seem to explain the differences in BSC at low and high frequencies. In fact, by varying the volume fraction from 0.05 to 0.5 for the theoretical BSCs of the OSA, only a small change in amplitude is observed on the theoretical BSCs (Fig 4(c)). The lack of agreement between BSCs at high and low frequencies is more likely due to a difference in the structures involved in diffusion. Indeed,

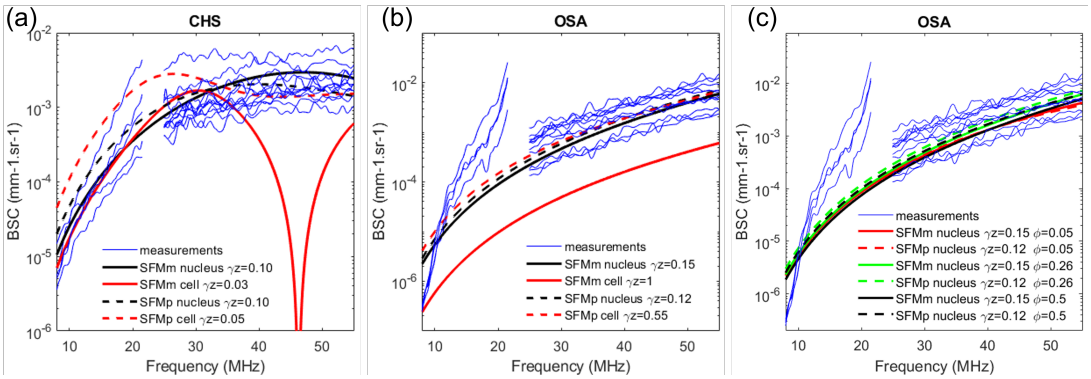

Fig. 4. Mean CHS (a) and OSA (b) BSCs obtained with the L228 and RMV704 probes. Theoretical BSCs using the monodisperse (SFMm) and polydisperse (SFMp) models using nucleus and cell values from histology are plotted using manually adjusted relative impedance contrast values. (c) Evolution of OSA theoretical BSCs using SFMm and SFMp for scatterer volumes fraction of 0.05, 0.26 and 0.5.

while the results suggest scattering by nuclei (Fig 4(b)) with high-frequency measurements, these are certainly too small (mean nucleus radius a=2.8 μm) to be involved in scattering at a frequency around 15 MHz ($ka \sim 0.17$).

Regarding the differentiation of OSA and CHS tumors, even though the amplitude and slope of the BSC for OSA and CHS are different at low frequency, the presence of a plateau in the CHS BSCs makes it easier to differentiate between these two tumor types at high frequency (Fig 4(a) and (b).

V. Conclusion

The use of low and high-frequency ultrasound scanning may provide additional information about the homogeneity of a tumor or the structures involved in ultrasound scattering. CHS and OSA tumors provided two examples of concordant and non-concordant BSCs at low and high-frequencies probably resulting from a difference in the structure involved in ultrasound scattering. This study demonstrates the interest of scanning at different frequencies for tumor characterization. Further experiments need to be implemented to assess the effect of tumor homogeneity on BSC using low and high-frequencies.

References

[1] M. L. Oelze and J. Mamou, "Review of Quantitative Ultrasound: Envelope Statistics and Backscatter Coefficient Imaging and Contributions to Diagnostic Ultrasound," *IEEE Transactions on Ultrasonics, Ferroelectrics, and Frequency Control*, vol. 63, pp. 336–351, Feb. 2016. Conference Name: IEEE Transactions on Ultrasonics, Ferroelectrics, and Frequency Control.

[2] E. J. Feleppa, T. Liu, A. Kalisz, M. C. Shao, N. Fleshner, V. Reuter, and W. R. Fair, "Ultrasonic spectral-parameter imaging of the prostate," *International Journal of Imaging Systems and Technology*, vol. 8, no. 1, pp. 11–25, 1997.

[3] J. Mamou, A. Coron, M. L. Oelze, E. Saegusa-Beecroft, M. Hata, P. Lee, J. Machi, E. Yanagihara, P. Laugier, and E. J. Feleppa, "Three-Dimensional High-Frequency Backscatter and Envelope Quantification of Cancerous Human Lymph Nodes," *Ultrasound in Medicine & Biology*, vol. 37, pp. 345–357, Mar. 2011.

[4] M. Oelze, W. O'Brien, J. Blue, and J. Zachary, "Differentiation and characterization of rat mammary fibroadenomas and 4T1 mouse carcinomas using quantitative ultrasound imaging," *IEEE Transactions on Medical Imaging*, vol. 23, pp. 764–771, June 2004.

[5] C. Malinet, B. Montcel, A. Dutour, I. Fajnorova, H. Liebgott, and P. Muleki-Seya, "Cancer characterization using light backscattering spectroscopy and quantitative ultrasound: an ex vivo study on sarcoma subtypes," *Scientific Reports*, vol. 13, p. 16650, Oct. 2023. Number: 1 Publisher: Nature Publishing Group.

[6] E. Franceschini and R. Guillermin, "Experimental assessment of four ultrasound scattering models for characterizing concentrated tissue-mimicking phantoms," *The Journal of the Acoustical Society of America*, vol. 132, pp. 3735–3747, Dec. 2012. Publisher: Acoustical Society of America.

[7] A. Han and W. D. O'brien, "Structure function for high-concentration biophantoms of polydisperse scatterer sizes," *IEEE Transactions on Ultrasonics, Ferroelectrics, and Frequency Control*, vol. 62, pp. 303–318, Feb. 2015. Conference Name: IEEE Transactions on Ultrasonics, Ferroelectrics, and Frequency Control.

[8] J. Perez, A. V. Decouvelaere, T. Pointecouteau, D. Pissaloux, J. P. Michot, A. Besse, J. Y. Blay, and A. Dutour, "Inhibition of chondrosarcoma growth by mtor inhibitor in an in vivo syngeneic rat model," *PLoS One*, vol. 7, no. 6, p. e32458, 2012.

[9] C. Khanna, J. Prehn, C. Yeung, J. Caylor, M. Tsokos, and L. Helman, "An orthotopic model of murine osteosarcoma with clonally related variants differing in pulmonary metastatic potential," *Clinical & Experimental Metastasis*, vol. 18, pp. 261–271, May 2000.

[10] R. Kuc, "Clinical Application of an Ultrasound Attenuation Coefficient Estimation Technique for Liver Pathology Characterization," *IEEE Transactions on Biomedical Engineering*, vol. BME-27, pp. 312–319, June 1980. Conference Name: IEEE Transactions on Biomedical Engineering.

[11] L. X. Yao, J. A. Zagzebski, and E. L. Madsen, "Backscatter coefficient measurements using a reference phantom to extract depth-dependent instrumentation factors," *Ultrasonic Imaging*, vol. 12, pp. 58–70, Jan. 1990.

[12] Y. Liu, A. G. Schwartz, Y. Hong, X. Peng, F. Xu, S. Thomopoulos, and G. M. Genin, "Correction of bias in the estimation of cell volume fraction from histology sections," *Journal of Biomechanics*, vol. 104, p. 109705, May 2020.

[13] J. Mamou, M. L. Oelze, W. D. O'Brien, and J. F. Zachary, "Identifying ultrasonic scattering sites from three-dimensional impedance maps," *The Journal of the Acoustical Society of America*, vol. 117, pp. 413–423, Jan. 2005. Publisher: Acoustical Society of America.

[14] M. N. Fadhel, E. S. Berndl, E. M. Strohm, and M. C. Kolios, "High-Frequency Acoustic Impedance Imaging of Cancer Cells," *Ultrasound in Medicine & Biology*, vol. 41, pp. 2700–2713, Oct. 2015.

[15] S. Leicht and K. Raum, "Acoustic impedance changes in cartilage and subchondral bone due to primary arthrosis," *Ultrasonics*, vol. 48, pp. 613–620, Nov. 2008.